Astron. Astrophys. 324, 1197–1205 (1997)

ASTRONOMY
AND
ASTROPHYSICS

Dust environment of Comet Hyakutake 1996B2

M. Fulle[1], **H. Mikuž**[2], **and S. Bosio**[1]

[1] Osservatorio Astronomico di Trieste, via G.B. Tiepolo 11, I-34131 Trieste, Italy
[2] University of Ljubljana, Department of Physics, Jadranska 19, SI-1000 Ljubljana, Slovenia

Received 13 December 1996 / Accepted 6 March 1997

Abstract. Narrow-band wide-field CCD images of the dust tail of Comet Hyakutake 1996B2 are analysed by means of the inverse dust tail model (Fulle 1989). The dust tail fits allow us to estimate the ejection velocity, mass loss rate and size distribution of the dust grains ejected during the months of March and April, 1996 (when the heliocentric distance was decreasing from 1.5 AU to 0.5 AU), in the size range between 1 μm and 1 mm. The best fits of the dust tail images are obtained for a power index of the velocity size dependence in agreement with classical models of the dust drag by gas in the inner coma (Gombosi 1986, Crifo 1991). The same fits do not show a clear dependence on the dust ejection anisotropy from the inner coma. The dust ejection velocity of 10 μm sized grains increases from about 50 m s^{-1} at the beginning of March, to about 500 m s^{-1} at the end of April. The mass loss rate increases from about 2 10^3 kg s^{-1} at the beginning of March, to about 10^4 kg s^{-1} in mid April. These loss rates depend linearly on the dust scattering efficiency (assumed equal to 1) and inversely on the albedo (assumed equal to 0.04). Twenty days before perihelion, both the size distribution power index and the mass loss rate show a strong drop, possibly due either to an increase of dust fragmentation processes inside the inner coma, or to a strong size dependence of the size distribution power index. The same time marks a difference in the observed dust environment, passing from a dust mass dominated by large grains to a dust mass dominated by small ones. The time averaged size distribution power index (equal to -3.6 ± 0.2) and the dust to gas ratio (at least one for the assumed dust albedo and scattering efficiency) point out that C/Hyakutake was a dusty comet. About 1% of the released dust mass goes to replenish the isotropic meteoric cloud (6 ± 3 10^3 kg of dust were injected into bound orbits).

Key words: comets: general – comets: individual: C/Hyakutake 1996B2 – meteoroids

1. Introduction

Comet Hyakutake 1996B2 was discovered at the end of January, 1996, and became the brightest comet of the last twenty years. Despite the short time available to well organize the observations, a lot of data was collected in the months preceding the perihelion, occurred on the 1st May, 1996. In this paper we focus our attention on the dust environment of this bright comet, taking into account narrow-band wide-field CCD images of the C/1996B2 dust tail. Dust tails maintain memory of the physical characteristics of the dust ejected during months preceding the observations, so that models able to extract from the images this information provide the time evolution of the comet dust environment. Comparisons of such results with the gas loss rate allow us to infer a fundamental parameter of the comet nucleus, i.e. its dust to gas ratio.

The dust tail model we adopt to analyse the available data is the inverse tail model developed by Fulle (1989), which was successfully tested on several comets (see Fulle 1996 and references therein). With respect to the original Finson-Probstein model (Finson & Probstein 1968), it presents two major advantages: (i) the fit of the input images is automatic, a fact ensuring us that the obtained fit is the best possible one, that the convergence criteria to the parameters allowing the best fit itself are objective, and that the model outputs are unique (in the least square fit sense); (ii) the analytical approach is substituted by a Monte-Carlo approach: the model dust tail is built-up by means of more than 10^6 sample particles, whose rigorous keplerian motion is computed, thus allowing us to avoid many limitations of the original method and to consider anisotropic dust ejections.

The free parameters of the model are the dust ejection velocity $v(t, d)$ from the inner coma (depending on the time, t, and the dust diameter, d), the power index u of the velocity size-dependence ($u = \frac{\partial \log v(t,d)}{\partial \log d}$), the time evolution of the size distribution and of the mass loss rate, and the dust ejection anisotropy; this is parametrized by the half-widht w of the dust ejection cone, whose axis points towards the Sun during all the comet orbital path. The fits of the GIOTTO-DIDSY data (McDonnell et al. 1991) by means of the fluence probabilistic model (Fulle et al. 1995) have shown that the best approximation of the cometary dust size distribution is a power law of the dust size. Therefore, the outputs of the adopted inverse model are the fits of the input images and the time evolutions of the dust velocity, size distribution power index and mass loss rate parametrized by sampled values of u and w.

Send offprint requests to: M. Fulle

Table 1. Log of observations. No, image number. UT, observation time (mid-exposure, April 1996). r, Δ, Sun-Comet and Earth-Comet distances (AU). λ, Earth cometocentric latitude on the comet orbital plane (degrees). α, phase angle (degrees). Exp, exposure time (sec).

No	UT	r	Δ	λ	α	Exp
0419RC4	19.806	0.447	0.847	21.4	97.0	300
0420RC1	20.803	0.422	0.880	21.5	94.4	180

2. Data Reduction

The wide-field CCD camera couples a photographic objective of 180 mm focal length to a CCD, having useful area of 353×540 pixel^2, thus covering a field of 2.45×3.75 square degrees, with a scale of 25 arcsec pixel^{-1}. Observations were performed at the Črni Vrh Observatory, Ljubljana (SL). Log of observations is reported in Table 1. Each CCD frame was flat-field and bias corrected. However, during the observations, performed less than two weeks before perihelion, the comet was placed in a rich star field very low on the horizon, with bright and variable background due to zodiacal light and twilight. Therefore, careful background subtraction and image calibration was necessary in order to extract from the CCD images the required photometrical data. In order to correct the changes of the background due to twilight and zodiacal light, a bilinear fit of the background was performed and subtracted, thus obtaining a new background constant over all the field within a few percent. The corrected background was adopted as a reference level of the surface light intensities of the tail, and was calibrated by means of standard stars available in both the considered frames.

The tail images were taken through an interference filter with passband centered on 647 nm and with FWHM of 10 nm (i.e., the reference continuum of H_2O^+ ion tail images), which is very close to the S photometric band of the Vilnius-Geneva photometric system, centered on 656 nm with FWHM of 19 nm (Straizys et al. 1982a). Despite its very short focal length, the adopted optical system provided wide point spread functions of all unsaturated stars, which covered boxes about 7 pixels wide. Therefore, precise absolute photometry was possible. As standard stars, we found in both the available frames two dwarf stars with high proper motion (Sandage & Kowal 1986) and with known spectral type. These facts allowed us to select the proper color index $V - S$ of both the standard stars and the Sun (Straizys et al. 1982b), and to convert all magnitudes to the Vilnius-Geneva photometric system. Residual photometric errors can be only due to the differences between the spectral types of the adopted standard stars and of the Sun, and can be estimated by the corresponding color index differences, which is 0.15 mag at most. It follows that the absolute values of the mass loss rates (the only quantity which is affected by this error source) are uncertain within the 15%, an error much lower than those intrinsic to the tail model.

For each image and standard star, we measured the brightness volume in a box of area A (arcsec^2) centered both on the star of magnitude S_S and on a nearby star-free sky area, thus obtaining the light intensities I_S and I_B, respectively. Then, the sky background S magnitude per arcsec^2 S_B is

$$S_B = S_S + 2.5 \log_{10} \frac{(I_S - I_B)A}{I_B} \quad (1)$$

The results shown in Table 2 point out that the image calibration error is always smaller than that due to the spectral differences between the standard stars and the Sun. The somewhat larger error of image 0419RC4 is due to the fact that the standard star G37-18 is placed in the outer dust tail itself, so that the sky background close to this star is affected by larger noise.

After calibration, each image was normalized to the same absolute brightness, in order to give consistent input data to the inverse tail model. Then, each image was rotated, in order to have the vertical axis parallel to the Sun-comet radius vector, and was median filtered, with a box larger than the star width, in order to remove from the tail image all the stars. Finally, the sky background level was subtracted from each image, which was resampled to the 30×30 pixel^2 format required by the inverse tail model. Such input images are shown in Figs. 1 - 4 for selected isophote values.

3. Results

During the observations, the Earth was close to the comet orbital plane (see the λ values in Table 1), and all the synchrones and the syndynes were confined in a tight angular sector centered on the nucleus. These perspective conditions are the most unfavourable for dust tail models, and this fact is reflected into the residual instability of the tail fits, which are shown in Figs. 1 - 4 for the parameter combinations reported in Table 3. We recall that the model fits the whole surface brightness of the dust tail in the sampled pixels of both images, and not only the shown isophotes. Therefore, it may occur that the fit is worse for some isophotes than for others. Moreover, the selection of the best fit must be evaluated by considering the fits of both images, in order to take into account the time evolution of the dust tail between the two considered observations. An objective evaluation of the fit quality is offered by the correlation index R (Table 3), which is the scalar product of the observed and reconstructed images. The correlation index in most sensitive to the errors related to the brightest pixels, exactly the contrary of an eye evaluation. The two highest R values are obtained for $u = -1/2$, so that the tail fits seem to contrain more the parameter u than w. The worse fits related to $u = -1$ are due to the much steeper radial increase of the dust shell sizes with respect to other u values, which makes unstable the convergence towards the fit.

This is the first time that the best tail fit is obtained for $u = -1/2$, which is in fact predicted by all hydrodynamical models of the dust drag by gas in the inner coma (Gombosi 1986, Crifo 1991). In Fig. 5 we plot the size interval of the dust grains composing the Hyakutake dust tail: it is mainly populated by micron-sized grains. Most dust tails analysed in the past by means of the inverse tail model were mainly populated by millimetric grains, and the best tail fits were provided by $u > -1/2$. The combination of these facts suggests the following conclusion. The dust velocity size-dependence is close to $u =$

Table 2. Image calibrations. No, image number. Star, standard star (Sandage & Kowal 1986) of magnitude V, color index $V-S$ and spectral type Sp. A, sky area (arcsec^2) over which the integrated intensities of the star I_S and of the near sky-background I_B were measured. S_B, surface magnitude of the sky background (S mag arcsec^{-2}).

No	Star	V	$V-S$	Sp	A	I_S	I_B	S_B
0419RC4	G37-10	8.38	0.65	K0V	30625	3419	2660	17.58
0419RC4	G37-18	9.49	0.72	K2V	30625	3175	2821	17.73
0420RC1	G37-10	8.38	0.65	K0V	30625	4764	3903	17.30
0420RC1	G37-18	9.49	0.72	K2V	30625	4418	4055	17.36

Table 3. Tail model input parameters and output results. $u = \frac{\partial \log v(t,d)}{\partial \log d}$. w, half-width of the Sun-pointing dust ejection cone. $\mathcal{N}_s$, tail model samples on each dust shell. $\mathcal{N}_\mu$, tail model size samples. $\mathcal{N}_t$, tail model time samples. N_t, dust mass loss rate samples. N_μ, size distribution samples. N_c, image cells. N_i, input images. $\mathcal{M}_t$, total released dust mass (10^5 kg). $\mathcal{M}_b$, dust mass injected into bound orbits (percentage of $\mathcal{M}_t$). R, correlation index between observed and reconstructed images.

u	w	$\mathcal{N}_s$	$\mathcal{N}_\mu$	$\mathcal{N}_t$	N_t	N_μ	N_c	N_i	$\mathcal{M}_t$	$\mathcal{M}_b$	R
-1/6	π	2578	100	150	15	10	900	2	5.3	3.3%	0.934
-1/6	$\pi/2$	1285	100	150	15	10	900	2	5.5	1.9%	0.924
-1/6	$\pi/4$	382	100	150	15	10	900	2	4.8	0.5%	0.955
-1/4	π	2578	100	150	15	10	900	2	5.3	3.0%	0.951
-1/4	$\pi/2$	1285	100	150	15	10	900	2	5.6	1.9%	0.937
-1/4	$\pi/4$	382	100	150	15	10	900	2	5.3	0.5%	0.926
-1/2	π	2578	100	150	15	10	900	2	2.9	1.0%	0.961
-1/2	$\pi/2$	1285	100	150	15	10	900	2	3.8	1.3%	0.957
-1/2	$\pi/4$	382	100	150	15	10	900	2	2.9	0.8%	0.939
-1	π	2578	100	150	15	10	900	2	1.3	1.0%	0.937
-1	$\pi/2$	1285	100	150	15	10	900	2	2.0	0.3%	0.939
-1	$\pi/4$	382	100	150	15	10	900	2	1.8	1.7%	0.902

$-1/2$ for micrometric grains, and between $u = -1/4$ and $u = 0$ for millimetric grains. This fact is consistent with photometry of Neck-Lines, which provides a direct measurement of the dust velocity of large grains (it resulted $u = -1/6$ for millimetric grains, Fulle & Sedmak 1988, Cremonese & Fulle 1989). The fit of the GIOTTO-DIDSY data (McDonnell et al. 1991) by means of the fluence probabilistic model (Fulle et al. 1995) provides an explanation of this u size-dependence. It was shown that the unexpected excess of the millimetric grain fluence observed by DIDSY may be due to a velocity dispersion independent of the dust size. It follows that the most probable velocity of small grains is much larger than its dispersion, so that the velocity size-dependence remains $u = -1/2$. On the contrary, the most probable velocity of large grains is lower than its dispersion, which in this case masks the original velocity size-dependence, so that $u \to 0$.

In Fig. 5 we plot the physical outputs related to the tail fits. In order to avoid confusion, we limit the plot to the outputs associated with the tail fits providing $R > 0.95$. In this way, it is possible to extract from Fig. 5 the physical behaviour common to the outputs related to the most significant fits. All the plotted dust ejection velocities show a strong dependence on the Sun-Comet distance r, close to 100 r^{-2} m s^{-1} (with r in AU) for grains of a 10 μm diameter. In steady conditions (coma gas cooling balanced by the solar heating, Delsemme 1982) the terminal gas velocity depends on $r^{-1/2}$. Gas drag models (e.g. Crifo 1991) showed that the dust ejection velocity from the inner coma is proportional to the terminal gas velocity. Therefore, we can conclude that the C/1996B2 coma was far from the steady state. This fact is most likely explained by strong changes in the dust ejection patterns due to seasonal variations, as it was shown by models of the 46P/Wirtanen coma (Crifo & Rodionov 1996). As it was found in all applications of the inverse tail model, the velocities related to stronger dust ejection anisotropies are larger than those related to isotropic ones (the velocities with $u = -1/2$, $w = \pi$ and $w = \pi/2$ overlap in Fig. 5). This fact is explained by the size of the dust shells building-up the dust tail: the more anisotropic the dust ejection, the smaller the sky projection of the ejected dust shell, so that larger ejection velocities are required to fit the tail width with anisotropic dust shells. Systematic differences are found between the velocities related to $u = -1/2$ and $u > -1/2$: these last velocities should be considered less probable, because the associated tail fits are worse. In particular, the tail models with $u = -1/6$ and $w = \pi/4$ show a much more extended sunward coma than observed, because they overestimate the velocity of the coma grains.

The dust mass loss rate shows an increase from two months to about twenty days before perihelion. The observation perspective (low Earth cometocentric latitudes, see Table 1) confined all the possible dust synchrones in a tight angular sector centered on the nucleus: the synchrone overlapping explains the well defined left hand side of the tail. For this reason, it was impossible to reconstruct the dust environment of the comet before the starting time shown in Fig. 5: the dust released before is

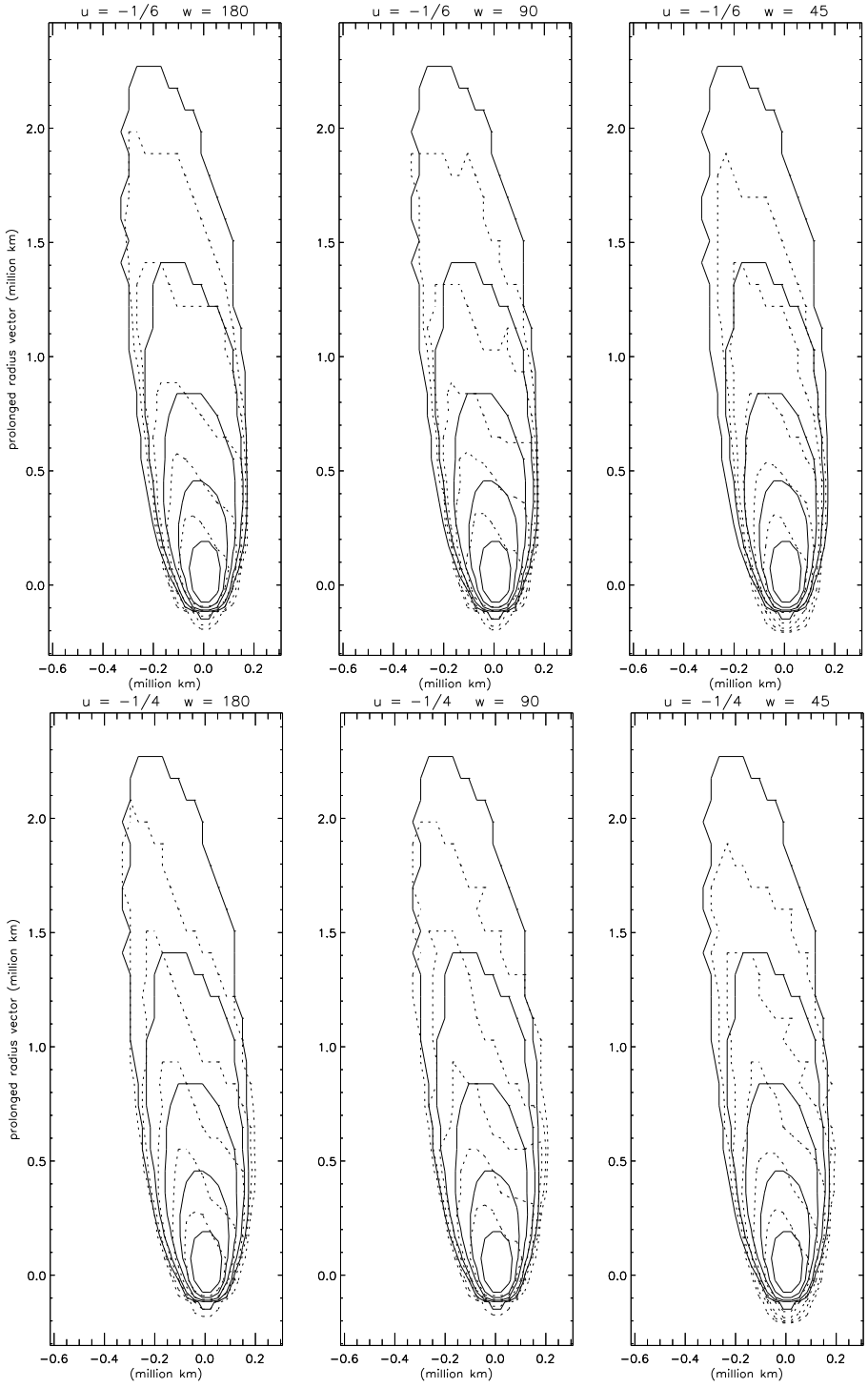

Fig. 1. Observed (continuous lines) and computed (dashed lines) image 0419RC4 of the dust tail of Comet Hyakutake 1996B2. The magnitude of the brightest isophote is 16.20 mag arcsec^{-2} in the S Vilnius-Geneva photometric system. The difference between isophotes is 0.75 mag (a factor 2 in surface light intensity). w is the half-width of the Sun-pointing dust ejection cone and $u = \frac{\partial \log v(t,d)}{\partial \log d}$.

masked by more abundant dust released after the time -60 days with respect to perihelion. The same synchrone overlapping introduces large uncertainty in the mass loss rate two months before perihelion, which strongly depends on the adopted parameter combination. When we take into account $u = -1/2$, which provides the two highest R values, the mass loss rate increases of a factor from three to ten, according to the w parameter. After the time -20 days, the size distribution power index shows a strong drop, which may point out a size dependence of the power index itself, since the observed size interval changes in time. However, the size interval change is limited to a size increase of a factor 4 only, so that most of the size interval (covering 2 decades) remains the same during the month preceding the perihelion. Therefore, the power index drop is consistent with a strong increase of dust fragmentation processes inside the coma during the comet approach to the Sun. If we exclude strong size dependences of the size distribution power index, the drop of the mass loss rate after the time -20 days can be correlated to

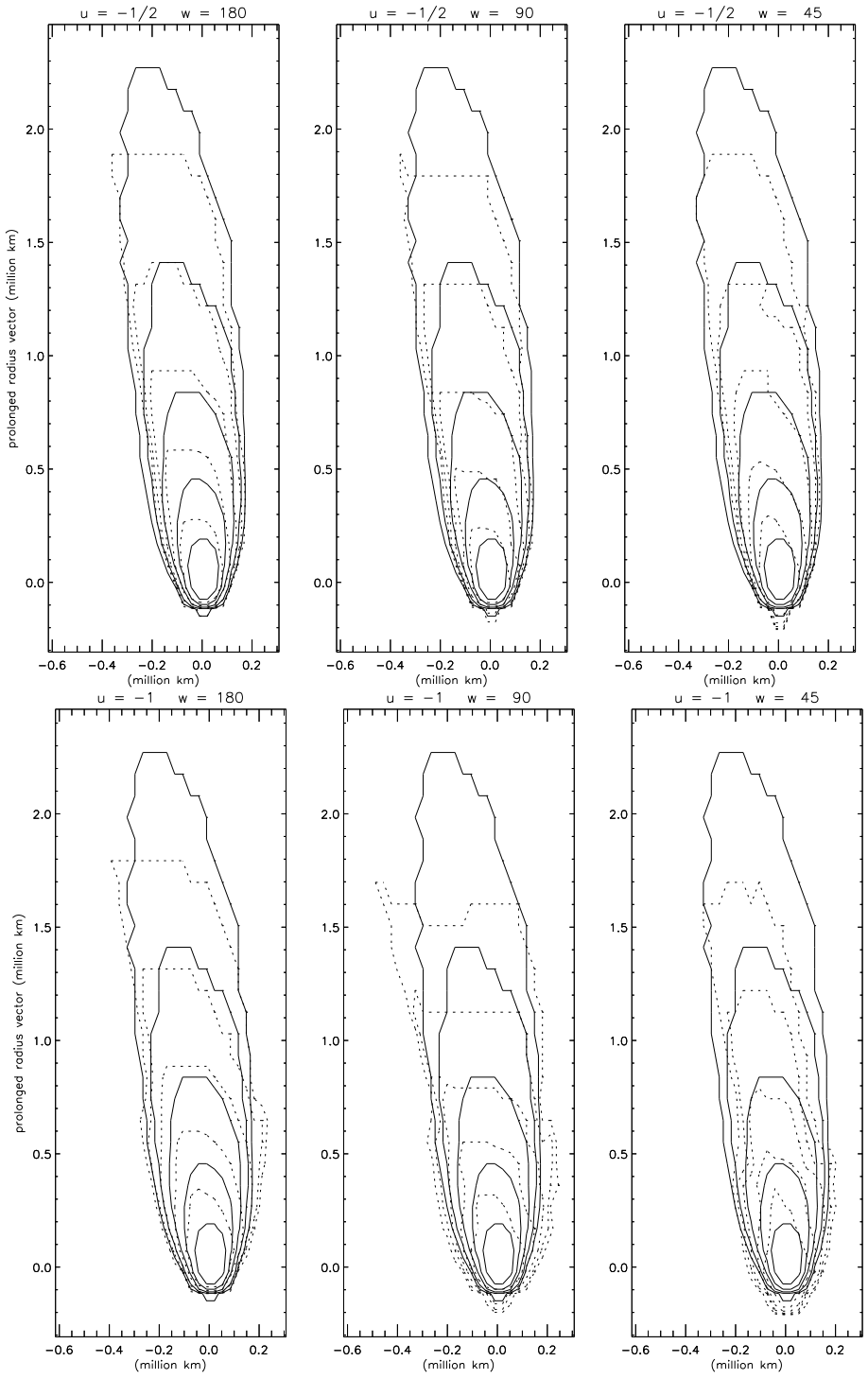

Fig. 2. Observed (continuous lines) and computed (dashed lines) image 0419RC4 of the dust tail of Comet Hyakutake 1996B2. The magnitude of the brightest isophote is 16.20 mag arcsec^{-2} in the S Vilnius-Geneva photometric system. The difference between isophotes is 0.75 mag (a factor 2 in surface light intensity). w is the half-width of the Sun-pointing dust ejection cone and $u = \frac{\partial \log v(t,d)}{\partial \log d}$.

the strong change of the dust size distribution at the same time: the mass loss rate is dominated by large grains before the time -20 days (the power index is larger than -4), whereas after the mass loss rate is dominated by smaller grains, with a probable mass loss rate decrease (the power index is smaller than -4).

We recall that the mass loss rates we obtain are lower limits of the real possible ones, because they refer to the shown limited size ranges shown in Fig. 5. In particular, large underestimates are possible when the power index is larger than -4, because in this case the release of unobserved meter-sized boulders would largely increase the mass loss rate. On the contrary, when the power index is smaller than -4, the release of unobserved submicrometric dust should not largely affect the mass loss rate. Obviously, if the power index at boulder sizes should be always much larger than -4, all the plotted mass loss rates would be lower limits only: the actual boulder population of comets is one of the open problems in comet physics.

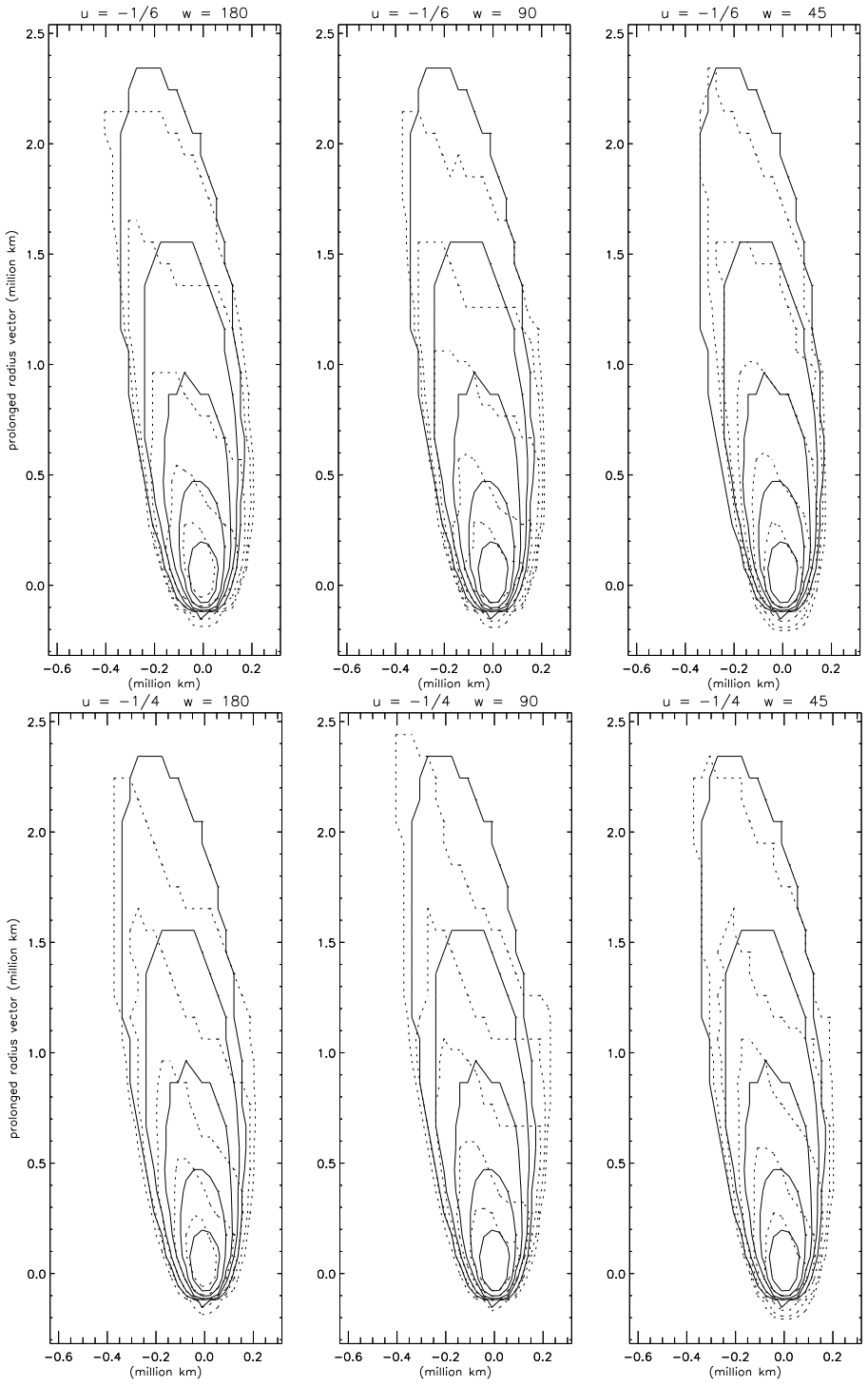

Fig. 3. Observed (continuous lines) and computed (dashed lines) image 0420RC1 of the dust tail of Comet Hyakutake 1996B2. The magnitude of the brightest isophote is 16.20 mag arcsec^{-2} in the S Vilnius-Geneva photometric system. The difference between isophotes is 0.75 mag (a factor 2 in surface light intensity). w is the half-width of the Sun-pointing dust ejection cone and $u = \frac{\partial \log v(t,d)}{\partial \log d}$.

4. Conclusions

Dust tail models allow us to obtain the best possible estimates of the dust to gas ratio of ground-based observed comets, because the long time spent by the dust to travel from the nucleus to the tail at Sun distances lower than 1 AU ensures us that all ices sublimated from the grains. On the contrary, coma observations do neither allow us to estimate the size of the observed grains, nor to verify whether the observed dust is heavily contaminated by ice. Unfortunately, all estimates of dust loss rates from optical observations depend on many poorly known parameters. However, dust tail models allow us to obtain loss rate estimates which depend on the lowest number of unknown parameters: the dust mass loss rate depends linearly on the dust scattering efficiency and inversely on the dust albedo. Only dust tail models provide mass loss rates independent of the poorly known dust bulk density (Finson & Probstein, 1968). Since the dust building-up the Hyakutake tail was released between 1.5 and 0.5 AU from the

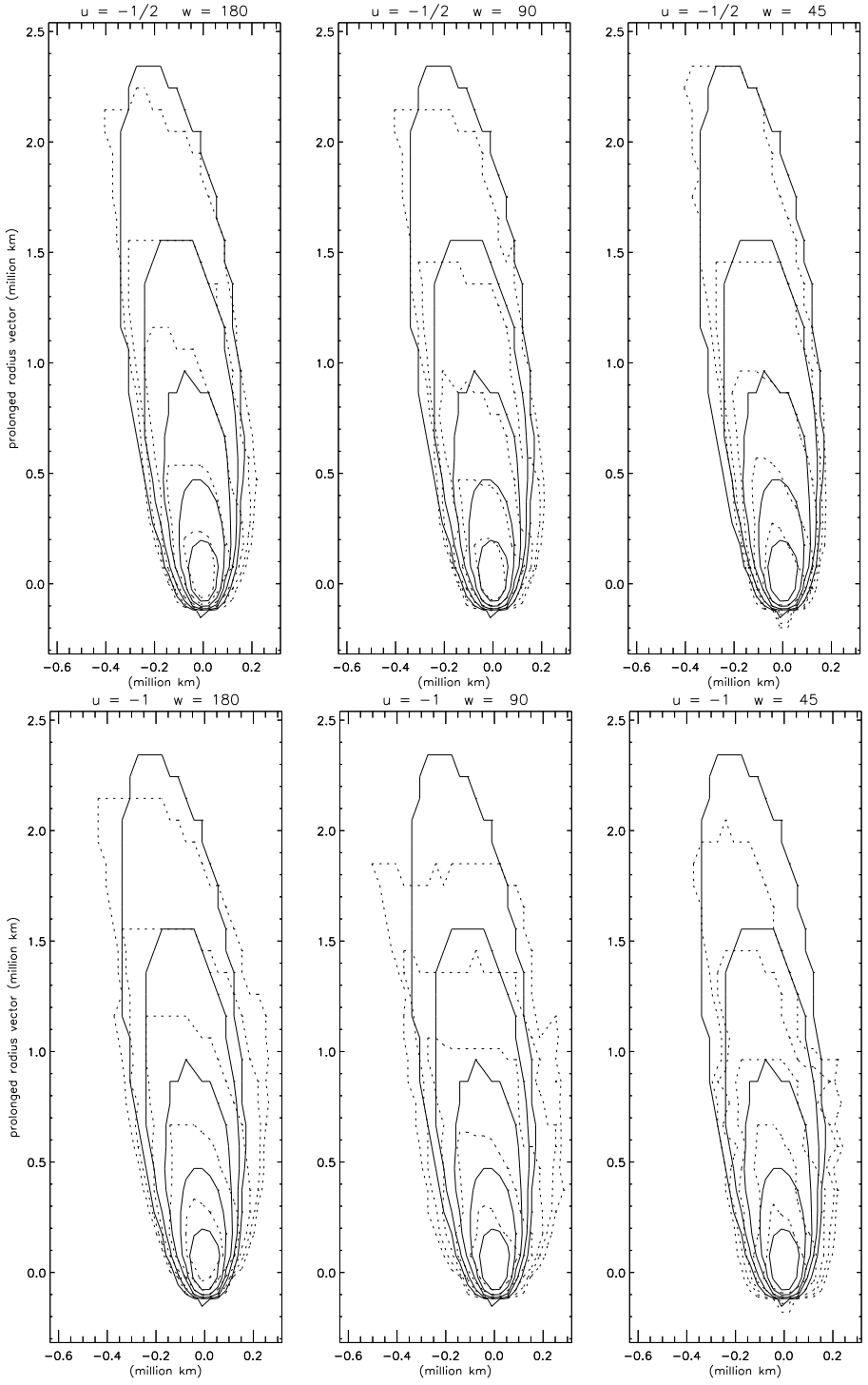

Fig. 4. Observed (continuous lines) and computed (dashed lines) image 0420RC1 of the dust tail of Comet Hyakutake 1996B2. The magnitude of the brightest isophote is 16.20 mag arcsec^{-2} in the S Vilnius-Geneva photometric system. The difference between isophotes is 0.75 mag (a factor 2 in surface light intensity). w is the half-width of the Sun-pointing dust ejection cone and $u = \frac{\partial \log v(t,d)}{\partial \log d}$.

Sun, we adopt an albedo equal to 0.04 (phase angles in Table 1) and a dust scattering efficiency equal to 1 (dark absorbing grains, Burns et al. 1979): changes of such adopted parameters would imply simple rescaling of the mass loss rates shown in Fig. 5 and of the estimated dust to gas ratio.

In order to estimate the dust to gas ratio of Comet Hyakutake 1996B2, we consider the water loss rate observations performed during March, 1996. Schleicher (1996a) and Festou et al. (1996a) report water loss rates close to 2 10^3 kg s^{-1} at the beginning of March, when the dust loss rate we obtain ranges from 10^3 to 4 10^3 kg s^{-1}. From 20th to 30th March, 1996, the water loss rate ranges from 3 10^3 to 10^4 kg s^{-1} (Schleicher 1996b, Festou et al. 1996b, Schleicher et al. 1996), when the dust loss rate we obtain ranges from 3 10^3 to 8 10^3 kg s^{-1}. When we take into account that tail models provide the best available underestimates of the dust mass loss rate from comets, we can conclude that the dust to gas ratio of this bright comet was at least one, as it was found for all comets whose dust tail was analysed by

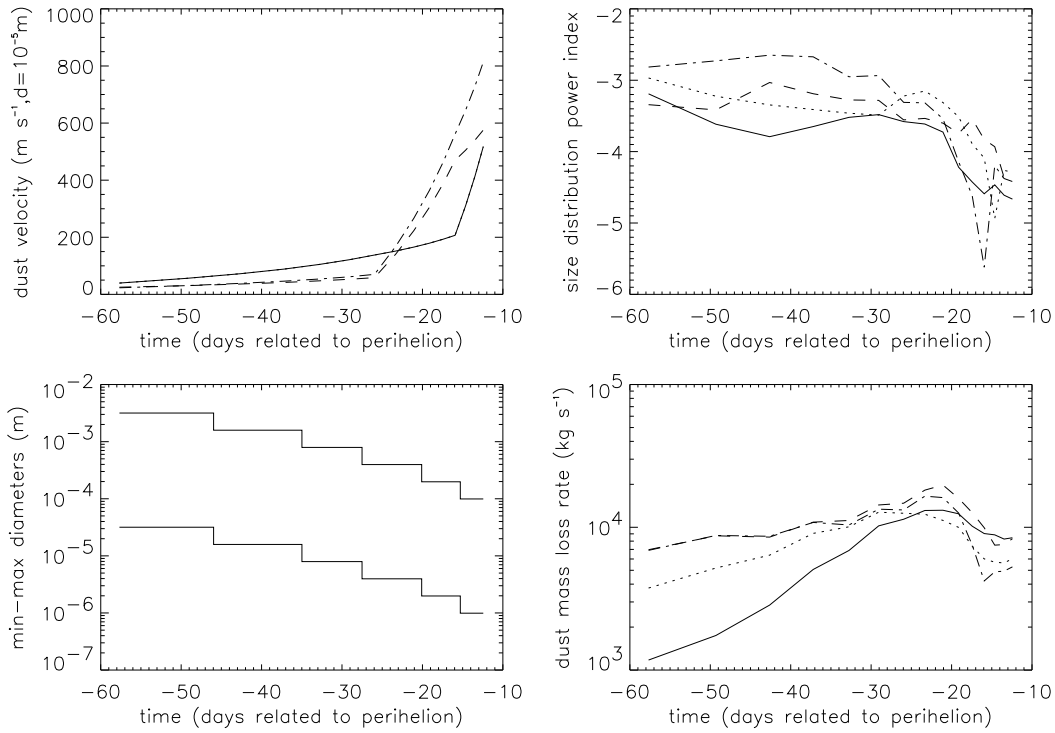

Fig. 5. Dust environment of Comet Hyakutake 1996B2 for the combinations of the free parameters with correlation index $R > 0.95$ (Table 3). The continuous lines refer to $u = -1/2$ and $w = \pi$, the dotted lines to $u = -1/2$ and $w = \pi/2$, the dashed lines to $u = -1/4$ and $w = \pi$ and the dotted-dashed lines to $u = -1/6$ and $w = \pi/4$, where $u = \frac{\partial \log v(t,d)}{\partial \log d}$ and w is the half-width of the Sun-pointing dust ejection cone. For each u-w combination, we plot the dust velocity, the mass loss rate, the power index of the differential size distribution and the time-dependent dust diameter interval to which all the physical quantities are related.

the adopted inverse model. The fact that C/Hyakutake is a dusty comet is confirmed by the power index of the time averaged size distribution, which results -3.6 ± 0.2. The Monte-Carlo procedure adopted by the inverse tail model computes the orbital eccentricity of each grain in the comet dust tail, thus allowing us to select the grains in bound orbits and to compute the dust mass which remains confined in our solar system. We obtain that a dust mass of $6 \pm 3\ 10^3$ kg was injected into bound orbits, going to replenish the isotropic meteoric cloud.

The time evolution of the dust environment of Comet Hyakutake 1996B2 is complex. All the output parameters show strong changes occurring about 20 days before perihelion: the dust ejection velocity shows a rapid increase, whereas the mass loss rate stops its increase and the size distribution power index strongly decreases, pointing out an evolution from a dust mass dominated by millimetric grains to a dust mass dominated by micrometric grains. A strong increase of fragmentation processes active in the inner coma is consistent with the changes both in the mass loss rate and in the size distribution. Realistic models of dust fragmentation in inner comae are extremely complex and not yet available (Crifo 1995): dust fragmentation implies gas release from the grains, i.e. changes of the dust gas interaction, which imply changes of the dust velocity, size distribution and mass loss rate. The observed changes of the model physical outputs might have been triggered by seasonal changes of the nucleus, which might have exposed new active spots to the sunlight after the 10th April, 1996. This might help to explain the strong increase of the dust ejection velocity too. Similar seasonal changes were invoked to explain the gas loss rate asymmetry with respect to perihelion of 1P/Halley (Weissman 1987), although many other physical processes (e.g. heat flow into the cometary crust, or heat release from the amorphous to crystalline ice transition, Rickman et al. 1984) cannot be excluded.

For comets 10P/Tempel 2 (Fulle 1996) and 2060 Chiron (Fulle 1994), dust tail models provided constraints to the nucleus spin state. In this case this is impossible, because the tail brightness distribution is not clearly correlated to the dust ejection anisotropy, and because the best fits are obtained for not strongly anisotropic dust ejections. The complexity of the dust environment evolution on long times (weeks) points out the difficulty of building-up realistic models of the long term behaviour of active cometary nuclei (which should mainly depend on nucleus seasons and heliocentric orbit), as well as it happens for models describing the evolution on short times (hours) of comet nuclei (which should mainly depend on nucleus spin and topography).

Acknowledgements. Standard stars were identified by means of the SIMBAD procedure, developed at the Observatoire Astronomique de

Strasbourg. An anonymous referee suggested significant improvements of a previous version of the paper.

References

Burns J.A., Lamy P.L., Soter S. 1979, Icarus 40, 1
Cremonese G., Fulle M. 1989, Icarus 80, 267
Crifo J.F. 1991, in Newburn R.L.Jr., Neugebauer M., Rahe J. (eds.), Comets in the Post-Halley Era, Kluwer, Dordrecht, 937
Crifo J.F. 1995, ApJ 445, 470
Crifo J.F., Rodionov A.V. 1996, Icarus (submitted)
Delsemme A.H. 1982, in Wilkening L.L. (ed.), Comets, The University of Arizona Press, Tucson, 85
Festou M., et al. 1996a, IAUC 6333
Festou M., et al. 1996b, IAUC 6355
Finson M.L., Probstein R.F. 1968, ApJ 154, 327
Fulle M. 1989, A&A 217, 283
Fulle M. 1994, A&A 282, 980
Fulle M. 1996, A&A 311, 333
Fulle M., Sedmak G. 1988, Icarus 74, 383
Fulle M., Colangeli L., Mennella V., Rotundi A., Bussoletti E. 1995, A&A 304, 622
Gombosi T.I. 1986, in: Battrick B. et al. (eds.), Exploration of Halley's Comet (Vol. 3), ESA SP-250, Paris, 167
McDonnell J.A.M., Lamy P.L., Pankiewicz G.S. 1991, in: Newburn R.L.Jr., Neugebauer M., Rahe J. (eds.) Comets in the Post-Halley Era, Vol. 2, Kluwer Academic Publisher, Dordrecht, 1043
Rickman H., Froeschle C., Klinger J. 1984, in: Klinger J., Benest A. Dolfus R, Smoluchowski R., (eds.) Ices in the Solar System, 419
Sandage A., Kowal C. 1986, AJ 91, 1140
Schleicher D. 1996a, IAUC 6333
Schleicher D. 1996b, IAUC 6344
Schleicher D. et al. 1996, IAUC 6372
Straizys V., Jodinskiene E., Hauck B. 1982a, Vilniaus Astronomijos Observatorijos Biuletenis 60, 50
Straizys V., Jodinskiene E., Hauck B. 1982b, Vilniaus Astronomijos Observatorijos Biuletenis 60, 16
Weissman P.R. 1987, A&A 187, 873

This article was processed by the author using Springer-Verlag LaTeX A&A style file *L-AA* version 3.